Geochimica et Cosmochimica Acta Vol. 49, pp. 2267–2279

0016-7037/85/$3.00 + .00

Accretionary rims on inclusions in the Allende meteorite

GLENN J. MACPHERSON[1], AKIHIKO HASHIMOTO and LAWRENCE GROSSMAN[2]
Department of the Geophysical Sciences, University of Chicago, 5734 S. Ellis Ave., Chicago, IL 60637

(*Received November* 27, 1984; *accepted in revised form July* 16, 1985)

Abstract—Many inclusions in Allende, particularly those with irregular shapes, are surrounded by a sequence of thin layers which differ from one another in texture, mineralogy and mineral-chemistry. The layer underlying all others contains either: IA, pyroxene needles + olivine + clumps of hedenbergite and andradite; IB, olivine doughnuts; or IC, rectangular olivine crystals. The next layer outward, II, contains tiny (<5 μm) olivine plates and Layer III large (5–10 μm) olivine laths. The final layer, IV, occurs as clumps of andradite + hedenbergite surrounded by magnesium-rich pyroxene needles. It separates Layer III from the Allende matrix which is more poorly sorted and more sulfide-rich than Layer III. Nepheline and iron sulfide are common constituents of most layers, the latter being particularly fine-grained and abundant in Layer II. Although not every layer is present on every inclusion, the sequence of layers is constant. Evidence that the rims are accretionary aggregates includes the presence of highly disequilibrium mineral assemblages and the fact that they are highly porous masses consisting of many euhedral crystals with few intergrowths. In addition, the layers are thickest in topographic hollows on the surfaces of inclusions and the inner layers are absent or discontinuous beyond such irregularities, suggesting that the probability of accretion of crystals was low initially, except in pockets, and became greater later, after a soft cushion of accreted condensate crystals had already formed. Separation of assemblages of different mineralogy, mineral-chemistry and texture into different rim layers seems best explained by nebular models in which long, slow cooling histories allow differentiation during condensation by grain/gas separation processes.

INTRODUCTION

SEVERAL WORKERS have noted the occurrence of unusually dark matrix-like material mantling peripheries of clasts, inclusions and chondrules in the Allende meteorite (GROSSMAN, 1975; FRULAND *et al.*, 1978; KING and KING, 1981). During the course of electron microscopic studies of refractory inclusions in Allende, we noticed that many of these objects have irregular rims around them that texturally resemble Allende matrix material but which differ slightly in grain size, modal mineralogy and mineral-chemistry (MACPHERSON and GROSSMAN, 1981). These rims are multilayered in many cases, and the innermost two or three layers form the dark mantles seen on slab surfaces and in thin sections. Our attention was attracted to these rims because their structures are similar to those of some terrestrial sedimentary rocks. In this paper, we present descriptions of the rim sequence on refractory inclusions only and interpret their possible origin and significance. In a preliminary report on these objects (MACPHERSON and GROSSMAN, 1981), we called them "clastic rims" which was not entirely appropriate since few of their constituent grains are fragments. KING and KING (1981) proposed the name "accretionary dark rims" for similar structures in several chondrites. We now also prefer the name "accretionary rims" for those in Allende because, as we shall show, their structures and mineralogical properties indicate they are primary accretion features that preserve evidence of aggregation processes in the solar nebula.

ANALYTICAL TECHNIQUES

Polished thin sections of all samples were examined with a JEOL JSM-35 scanning electron microscope (SEM), equipped with a back-scattered electron (b.s.e.) detector and a Si(Li) X-ray analyzer. Mineral analyses were obtained with the latter device, using an on-line PDP 11/03 computer for data reduction *via* a program based on the procedure of BENCE and ALBEE (1968). Natural and synthetic minerals and glasses were used for standards.

Bulk analyses of individual rim layers were obtained using an ARL-SEMQ nine-spectrometer automated electron microprobe by electronically scanning the beam over representative areas (~100 × 100 μm) of rim layers on each inclusion. Data were reduced using the method of BENCE and ALBEE (1968) and correction factors of ALBEE and RAY (1970). Analyses of standards by this technique showed no loss of accuracy due to Rowland circle effects. No corrections were made for heterogeneity because the grain size in these layers approaches that for the "homogeneous correction" case (*e.g.*, ALBEE *et al.*, 1977). No corrections were made for porosity but, rather, the analyses were simply normalized and used only for comparison purposes.

DESCRIPTIONS

Accretionary rim structures are present on nearly all refractory inclusions, fine-grained as well as coarse-grained, in our collection. An example is shown in Fig. 1, a b.s.e. photomicrograph (a) and line drawing (b) of a portion of the outer surface of an irregularly-shaped fluffy Type A inclusion (MACPHERSON and GROSSMAN, 1984) labelled TS24F1. Two important features of accretionary rims are seen. First, these rims are multi-layered. The individual layers, delineated schematically in Fig. 1b, are distinguished from each other and from "normal" Allende matrix by grain size, modal mineralogy and mineral chemistry. Second, rim material is invariably thickest in topographic depressions on the surfaces of inclusions. Note how each individual

[1] Present address: Smithsonian Institution, Department of Mineral Sciences, Washington, D.C. 20560.
[2] Also the Enrico Fermi Institute.

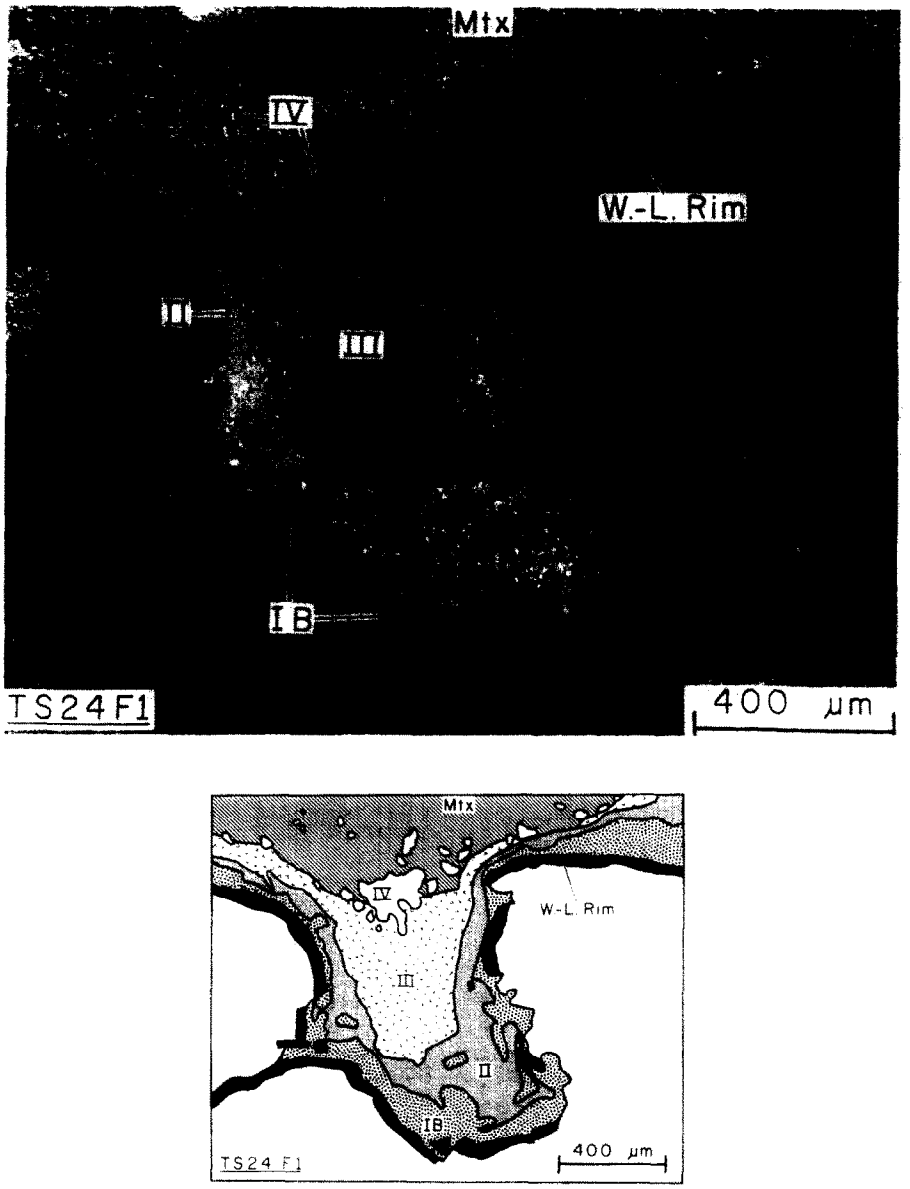

FIG. 1. B.s.e. photomicrograph (a) and line drawing (b) of a pocket on the surface of the "fluffy" Type A inclusion TS24F1. The pocket is filled by four accretionary rim layers, each of which thins drastically towards the outside of the pocket. The innermost layer (IB) consists of blocky olivine; the bright second layer (II) is very fine-grained olivine plus sulfide; the third layer (III) is coarser olivine with less sulfide; Layer IV consists of clumps of andradite + hedenbergite (white) mantled by magnesium-rich pyroxene needles (dark). Note that the normal Allende matrix (Mtx) is much richer in large sulfide granules than any of the accretionary rim layers. The Wark-Lovering (W.-L.) rim maintains uniform thickness.

layer in Fig. 1 preferentially fills the pocket on the surface of the inclusion but thins markedly at the edges of the pocket. This universal property of accretionary rims is of major importance in interpreting their origin. Figure 1 also shows that the accretionary rim overlies not only the melilite-rich refractory assemblage in the interior of the inclusion but also the thin, multi-layered Wark-Lovering (1977) rim sequence. The mineralogy and textures of the latter are completely unlike those of accretionary rims and are interpreted to have a different origin (MACPHERSON *et al.*, 1981). Similarly, the mineralogy, texture, occurrence and, consequently, origin of the objects referred to by RUBIN (1984) as "coarse-grained chondrule rims" in Allende are quite different from the objects described herein.

There is a consistent sequence of layers within the accretionary rims from one refractory inclusion to another. An idealized sequence is shown in Fig. 2. Although most inclusions do not possess the complete sequence of layers, the relative "stratigraphic position" of the layers that are present remains the same. Most commonly, it is one or more of the inner layers that

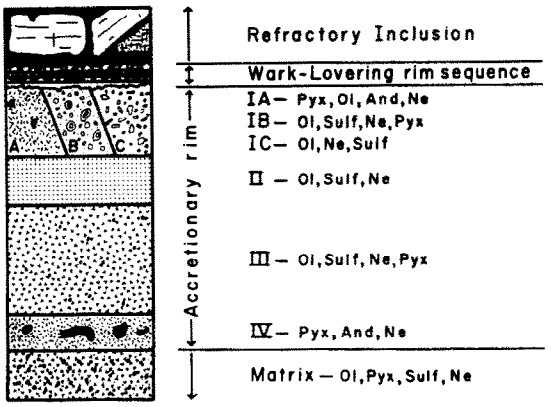

FIG. 2. Idealized stratigraphic section of a complete accretionary rim sequence.

are missing. Following are descriptions and close-up photomicrographs of each of the layers in succession, starting with the innermost (I) and ending with the Allende matrix.

Layer I

This refers collectively to three mineralogically- and texturally-distinct layers which, if present, underlie all other layers. Although more than one of the three may occur on any particular inclusion, we have never seen them in contact with one another and are thus uncertain about their positions in the sequence relative to one another. Each of the layers is discontinuous and, generally, is found only in topographic depressions on the surfaces of inclusions.

Figure 3 is a b.s.e. photomicrograph illustrating one layer, IA, that fills a re-entrant on the surface of inclusion TS10F1 (MACPHERSON *et al.*, 1981). On this inclusion, the layer is up to 0.4 mm thick in the center of deep pockets but nearly non-existent elsewhere. It consists mostly of tiny pyroxene needles having a wide range of composition from salite (En30–35 Fs15–20 Wo~50) to hedenbergite (Fs50 Wo50), with lesser and variable proportions of olivine (Fo~55–70) as well as nepheline and sulfide. The pyroxene contains up to 3% Al_2O_3. ALLEN *et al.* (1978) first described material belonging to this layer on the surface of the fluffy Type A inclusion CG-11. Note the characteristic feature here, and in other layers described below, of euhedral crystals packed loosely together with little evidence of intergrowths between them. Interstitial areas are either void or filled with nepheline, which is sometimes intergrown with pyroxene. Scattered within this layer are clumps of hedenbergite and andradite which also appear to be loosely enclosed within the pyroxene needle aggregate. As shown below, this occurrence of hedenbergite-andradite clumps within a matrix of more Mg-rich pyroxene needles is identical to Layer IV except that, in the latter, the volume of pyroxene needles is minor compared with the iron-rich clumps. This disequilibrium assemblage of magnesium-rich pyroxene in direct contact with hedenbergite, and the porous loosely-packed texture, are evidence that this layer originated as a loose aggregate of independently-formed crystals, as discussed later.

Details of Layer IB are shown in Fig. 4 and more general views in Figs. 1 and 8. This layer is as thick as 0.5 mm in pockets on some inclusions but is 100 μm or less elsewhere on the surfaces of the same inclusions. It consists mostly of blocky olivine crystals (up to 100 μm), abundant interstitial void space and lesser amounts of pyroxene, sulfide and nepheline. Many olivine grains appear to be hollow, "doughnut-shaped" single crystals but optical examination with a polarizing microscope shows that the rings are actually composed of many crystals. The cores of some of these doughnuts contain grains of sulfide and/or metal, while others are

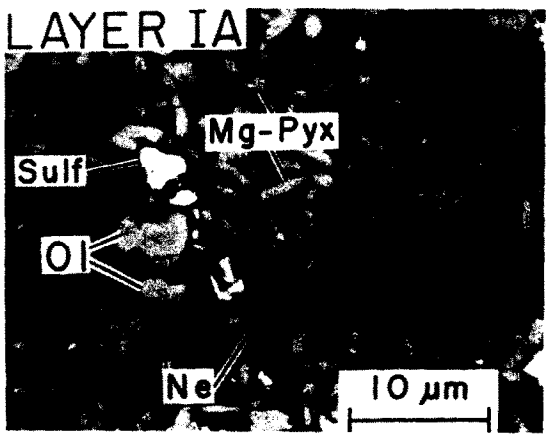

FIG. 3. Close-up b.s.e. photomicrograph of rim Layer IA on inclusion TS10F1. Loosely-packed needles of magnesium-rich clinopyroxene (Mg-Pyx) coexist with lesser olivine (Ol), iron sulfide (Sulf) and nepheline (Ne; dark grey). Interstices are void (black).

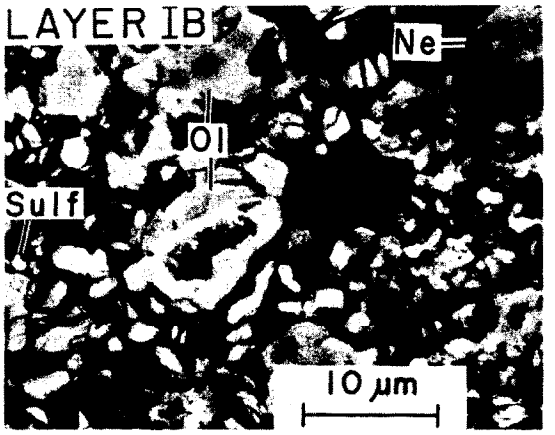

FIG. 4. Close-up b.s.e. photomicrograph of rim Layer IB on inclusion TS24F1. Blocky olivine grains, some doughnut-shaped, are loosely packed together with minor sulfide and nepheline. Interstices are void (black). Abbreviations as in Fig. 3.

hollow. Such structures are very similar to olivine structures in amoeboid olivine aggregates described by BAR-MATTHEWS *et al.* (1979). Olivine in Layer IB ranges in composition from Fo~56 to Fo94. The larger crystals are zoned and, as indicated by albedo variations in Fig. 4, the outer parts of such crystals are more iron-rich than the cores. Pyroxene in this layer ranges in composition from En25 Fs25 Wo50 to En35 Fs15 Wo50 and contains 1.0–1.5% Al_2O_3 on average.

Layer IC contains small (≤10 μm) olivine crystals which are rectangular in cross-section, differing in shape from both the blocky olivine crystals described above and from the spindle-shaped olivine crystals common in the Allende matrix and outer rim layers described below. An enlarged b.s.e. photomicrograph of Layer IC from the rim on the so-called "sinuous inclusion", TS10F1, illustrated by MACPHERSON *et al.* (1981) is shown in Fig. 5. The olivine crystals shown have the approximate composition Fo66, which is typical of grains in this layer. Olivine grains in the rim of the isotopically-unusual inclusion HAL (J. M. ALLEN *et al.*, 1980) also have rectangular cross-sections and fall in the range Fo66–78. Like these, the ones in the sinuous inclusion rim have enclosed submicron-sized grains of an aluminum-rich phase, visible as dark specks in Fig. 5. The grains are too small for certain identification, but the presence of sodium in their X-ray spectra suggests they may be nepheline. These olivine crystals are loosely packed in a matrix consisting largely of nepheline which is both interstitial to and intergrown with the olivine. Sulfide and Ni-Fe metal are accessory phases.

The three variants of Layer I thus differ from one another either in mineralogy (pyroxene in IA *vs.* olivine in IB and IC) or in crystal shape (blocky olivine in IB *vs.* rectangular olivine in IC).

Layer II

Layer II, like Layer I, is encountered most commonly in topographic depressions on the surfaces of inclusions where it can be up to 150 μm thick, but rarely can be found as a more extended but thinner (50–70 μm) layer beyond such depressions.

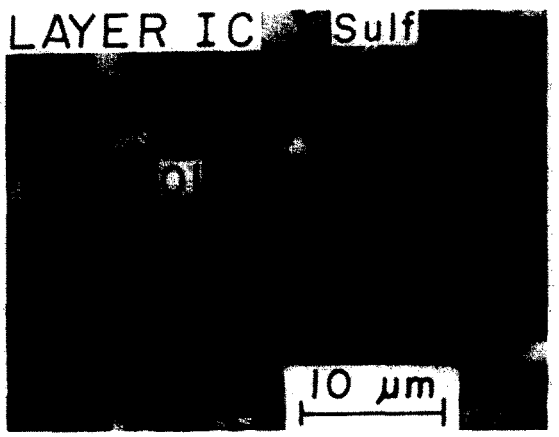

FIG. 5. Close-up b.s.e. photomicrograph of rim Layer IC on inclusion TS10F1. Rectangular olivine crystals coexist with abundant nepheline (not visible) and accessory sulfide. Tiny dark specks inside olivine crystals contain Na and Al. Abbreviations as used previously.

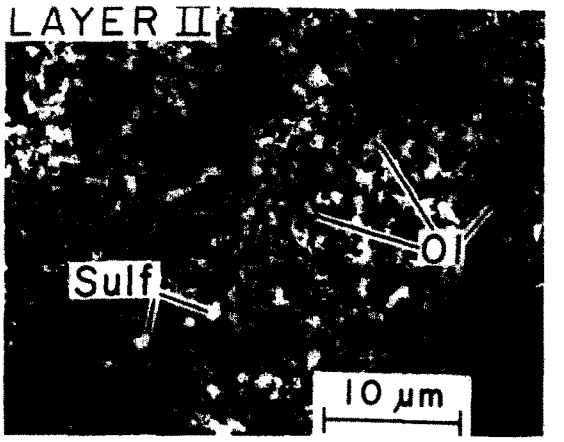

FIG. 6. Close-up b.s.e. photomicrograph of rim Layer II on inclusion TS24F1. Note the very tiny average grain size of the olivine crystals. In addition to the relatively large sulfide granules, there is also very abundant sulfide dust that partially fills interstices between olivine crystals. This dust is just visible in the photo as bright specks, and its abundance contributes to the overall high electron albedo (brightness) seen in Fig. 1. Abbreviations as used previously.

Layer II consists primarily of tiny (up to ~5 μm, but most are much smaller), euhedral olivine plates having the composition Fo~52–65 (Fig. 6). Interstitial to these olivine crystals are void space, feldspathoids and sulfides. Pyroxene (En24 Fs26 Wo50) is a very minor phase in this layer and contains 1.2–1.5% Al_2O_3. Although a few relatively large (~1–5 μm) grains of sulfide are visible in Fig. 6, most sulfide in this layer is present as exceedingly tiny (≪1 μm) grains that are barely visible in the photo. The hallmark of Layer II is its very small average grain size compared with the other layers, particularly Layer III which is mineralogically and texturally identical except for being much coarser on average. Note that Layer II is a porous meshwork of euhedral crystals and, in this respect, is similar to Layer IA. These tiny, euhedral olivine plates show neither intergrowths with neighboring crystals nor growth interference textures, *e.g.* crystals terminating at the sides of other crystals.

Layer III

Layer III is the most continuous of all layers. Although it, too, is thickest (up to 540 μm) in pockets on the surfaces of inclusions, it can generally be traced as a 50 to 100 μm thick layer around most of the perimeter of any given inclusion.

Layer III (Fig. 7) texturally resembles Layer II but, as already noted, contains a much higher proportion of larger (5–10 μm) olivine crystals than Layer II. A comparison of the two layers is shown in Fig. 8, a photomicrograph of the contact between Layer II and Layer III on inclusion TS24F1 (Fig. 1). Compositions

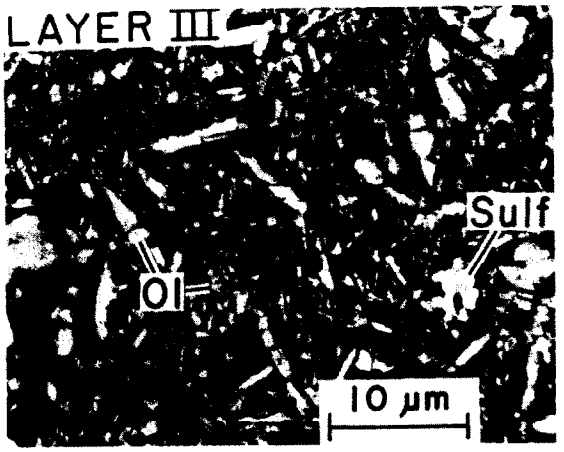

FIG. 7. Close-up b.s.e. photomicrograph of rim Layer III on inclusion TS24F1. Although mineralogically similar to Layer II in Fig. 6, this layer has much coarser average grain size and lacks the abundant sulfide dust. Abbreviations as used previously.

of olivine crystals in Layer III commonly lie in the range Fo55–65, but a few large crystals may have cores up to Fo~83. Pyroxene is a minor phase in this layer, ranges in composition from En32 Fs18 Wo50 to En22 Fs28 Wo50 and contains 0.5–3.5% Al_2O_3. Sulfide is present only as micron-sized or larger grains. The abundant and extremely fine-grained sulfide dust of Layer II is absent. Layer III is the thickest and most commonly encountered of the accretionary rim layers. On some inclusions, part or all of Layer III is very dark in transmitted light, corresponding to the dark mantles seen on slab surface. On other inclusions, it is not dark and on still others, the outer part of Layer III is dark and the inner part is not. In the latter inclusions, we have been unable to detect any significant difference in mineralogy, texture or chemical composition (Table 1) capable of accounting for the color variation. As shown below (see Bulk Chemistry), dark portions of these rims owe their appearance to an element not generally analyzed for, possibly carbon.

Layer IV

This layer (Fig. 9) generally occurs as clumps and stringers of material separating the inner accretionary layers from the Allende matrix. This layer is thin (~50 μm) and rarely continuous, although we have observed it to be continuous with a thickness of up to ~250 μm on one inclusion. Layer IV consists of clumps (up to ~100 μm) of andradite and iron-rich pyroxene embedded in a meshwork of tiny (<10 μm), euhedral, Mg-rich pyroxene needles. The clumps are composed mostly of andradite and hedenbergitic pyroxene, with minor more magnesium-rich pyroxene and wollastonite. Wollastonite contains ~2% FeO and occurs either as individual plates (5–20 μm long) or as 50 μm clumps of plates usually in contact with andradite but occasionally in direct contact with hedenbergite (En3 Fs46 Wo51). Minor amounts of feldspathoids and sulfide are found among the pyroxene needles. Stringers and patches of Layer IV are, in turn, partially enclosed by Allende matrix material or, in some places, by Layer III. Layer IV is mineralogically and texturally similar to Layer IA and differs from the latter only in having a much smaller volume of magnesium-rich pyroxene needles surrounding the andradite-hedenbergite clumps. Layers IA and IV can be found on the same inclusion, separated from one another by olivine-rich Layers II and III.

The range of pyroxene compositions within a given Layer IA is the same as that found within a typical example of Layer IV. Within a few microns of each other in a single andradite-hedenbergite clump can be found pyroxene grains as different in composition from one another as En1 Fs48 Wo51 and En32 Fs14 Wo54. The latter composition is typical of pyroxene needles that surround the clumps. In all grains we have analyzed, Al_2O_3 is less than ~6% (most <3%) and TiO_2 is below the limit of detection for energy dispersive analysis. The tremendous spread in the Fe/Mg ratio of pyroxene is the most remarkable feature of both Layers IA and IV, and indicates a highly disequilibrium assemblage. Such assemblages place strong constraints on the temperatures at which these rims could have been assembled or subsequently heated, as discussed below.

The boundary between Layer III and the Allende matrix, as demarcated by the presence of Layer IV, is the most easily recognizable feature of accretionary rims. Provided that the thin sections are thin enough, this boundary can even be seen optically in transmitted light because the coarser-grained clumps in Layer IV are pale green in color and birefringent, and separate the poorly-sorted Allende matrix (see below) from the uniformly dark and better-sorted inner layers.

Allende matrix

The Allende matrix (Fig. 10) is composed predominantly of euhedral olivine plates (mostly 1–5 μm in

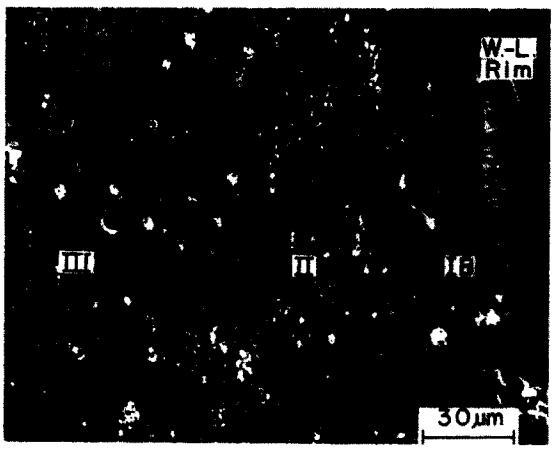

FIG. 8. B.s.e. photomicrograph showing a comparison of rim Layers IB, II and III on the surface of TS24F1. The difference in grain size between Layers II and III is readily apparent, as are the blocky olivines in Layer IB. Abbreviations as used previously.

Table 1. Bulk Compositions of Accretionary Rim Layers on Allende Inclusions.

Inclusion	TS24F1				TS25F1				TS65F1		TS19F1			
Rim Layer	IB	II	III	Mtx	IB	III inner dark	III outer light	Mtx	III	Mtx	II dark	III dark	III light	IV
	1	2	3	4	5	6	7	8	9	10	11	12	13	14
SiO_2	39.67	31.32	33.86	34.62	36.58	34.74	35.62	36.22	35.20	33.93	29.42	31.70	34.00	42.43
Al_2O_3	4.79	3.14	3.65	2.94	.82	2.69	2.86	2.84	3.55	2.53	4.81	5.27	6.20	3.42
FeO[1]	20.99	28.92	28.87	29.61	26.92	27.91	29.45	28.97	31.26	32.94	33.42	32.14	30.88	19.43
MgO	22.96	25.14	26.91	22.56	30.67	27.48	24.50	21.44	21.59	20.65	20.34	22.56	20.64	10.96
CaO	7.19	1.77	1.80	4.15	1.78	2.70	3.10	4.99	2.57	3.70	1.38	.90	2.63	19.60
K_2O	.18	.10	.08	.09	.06	.05	.08	.09	.17	.10	.06	.09	.10	.05
Na_2O	1.32	.38	.26	.14	.10	.21	.35	.34	1.17	.21	.38	.79	.99	.16
FeS[1]	.75	3.09	1.49	2.29	.29	1.01	.77	1.61	1.49	3.10	5.16	2.86	1.71	1.42
NiS[1]	.66	4.64	1.58	2.09	1.28	1.71	1.76	2.01	1.51	2.34	3.54	2.20	1.35	1.05
Total, norm.[2]	98.51	98.50	98.50	98.49	98.50	98.50	98.49	98.51	98.51	98.50	98.51	98.51	98.50	98.52
(Orig.)	(84.13)	(88.55)	(84.18)	(83.99)	(87.91)	(85.01)	(87.08)	(84.91)	(88.20)	(86.00)	(86.47)	(84.52)	(82.33)	(84.67)
Number of Analyses	3	5	4	1	5	5	7	7	8	5	11	4	3	2
AMOUNT PRESENT (%)														
Olivine	60.4	82.4	87.6	78.2	90.5	84.4	82.1	73.5	79.6	81.9	82.7	86.4	79.9	---
Pyroxene	30.0	7.2	7.6	16.4	7.3	11.5	13.1	20.7	10.3	11.2	5.7	3.3	10.6	56.5
Nepheline	8.1	2.3	1.6	0.9	0.6	1.3	2.1	2.1	7.1	1.3	2.4	4.9	6.2	---
Total Sulfides	1.5	8.0	3.2	4.6	1.6	2.8	2.6	3.8	3.1	5.6	9.2	5.3	3.2	4.0
Andradite	---	---	---	---	---	---	---	---	---	---	---	---	---	39.6
MOLAR FeO/FeO + MgO														
Pyroxene[4]	.48	.51	.51	.58	.42*	.42*	.42*	.47*	.42*	.47*	.56	.35	.35	.61
Olivine	.32	.39	.37	.41	.33	.36	.40	.43	.45	.47	.48	.45	.46	---
EXCESS Al_2O_3	1.75	2.27	3.00	2.54	0.42	2.02	1.86	1.94	0.93	1.99	3.95	3.60	4.02	2.29

size, some up to 20 μm) and fragments thereof with lesser amounts of clinopyroxene, sulfides and feldspathoids. Most olivine is Fo~50–60 in composition, but some larger, zoned grains have cores of Fo80–85. Pyroxene ranges in composition from En32 Fs18 Wo50 to En21 Fs29 Wo50 and contains 0.8–1.5% Al_2O_3. One feature evident from Fig. 1 is that *large* (up to 10 μm) sulfide grains are much more abundant in the normal Allende matrix than in any of the accretionary rim layers. Sulfide is more abundant in Layer II than in the matrix but is very fine-grained. This enrichment is also evident in the bulk composition of the matrix relative to that of rim layers, as shown in Table 1 and discussed below. In addition, the matrix is more poorly-sorted in its grain size relative to the rim layers, containing abundant large (>20 μm) olivine crystal fragments, polycrystalline aggregates of equant olivine grains and fragments of inclusions of various types. This poorly-sorted aspect of the Allende matrix relative to the rim layers is particularly visible in transmitted light. Another distinguishing characteristic of the Allende matrix is that the spindle-shaped olivine crystals in the latter are larger than those in Layer II and different in shape from olivine crystals in IB and IC. Although Layer III (Fig. 7) is very similar in texture and grain size to the matrix, the two are distinguished by the poorer sorting and sulfide enrichment of the matrix. In spite of these differences, however, the general textural and mineralogical similarity between the Allende matrix and the rim layers indicates they share a common origin. In a sense, the Allende matrix can be considered an outermost "super" rim layer that encloses everything else in the meteorite (see Discussion).

BULK CHEMISTRY

Major element compositions of 19 rim layers on nine different coarse-grained inclusions and of the matrix just outside of the rim layers on seven of these inclusions are given in Table 1, along with a wet chemical, bulk analysis of the Allende matrix by CLARKE *et al.* (1970). In the case of five layers, inner and outer portions could be distinguished on the basis of color, were analyzed individually and their compositions reported separately on Table 1. Also shown is the number of rastered beam analyses that were averaged together to obtain each column of data. In order to facilitate comparison, the microprobe and wet chemical analyses have all been recalculated to show total nickel as NiS, the remaining sulfur as FeS and all remaining iron as FeO. In addition, microprobe analyses have been normalized to 98.5%, the approximate sum of those components in the wet chemical analysis that were also analyzed by microprobe.

The seven matrix analyses are generally in good agreement with one another, especially considering the relatively small areas represented by each. The sample of material used in the wet chemical analysis of CLARKE *et al.* (1970) was obtained by sieving to remove the coarsest fraction from a crushed sample of the bulk meteorite. Although the wet chemical method is more

Table 1. Bulk Compositions of Accretionary Rim Layers on Allende Inclusions

TS45F1			TS4F1		NMNH 3643					TS10F1			
IA inner dark	IA outer light	Mtx	III dark	Mtx	IA	IB	III	IV	Mtx	IA inner	IA outer	IV	Mtx
15	16	17	18	19	20	21	22	23	24	25	26	27	28
45.81	46.41	34.33	31.71	33.78	44.05	39.03	33.01	46.21	33.80	40.94	39.34	43.75	33.80
3.80	3.32	2.50	5.07	2.61	11.42	5.82	4.45	2.41	2.92	7.33	4.82	2.19	3.45
12.36	11.89	31.60	36.43	32.28	12.93	19.55	32.33	16.72	33.31	15.09	23.37	18.40	33.12
14.17	12.63	21.42	22.30	16.94	5.09	16.20	22.06	8.47	20.80	14.52	16.21	8.13	20.82
20.06	22.01	3.50	.84	6.54	24.43	11.95	2.27	22.66	3.41	15.88	10.66	23.75	3.66
.04	.04	.05	.08	.03	.03	.02	.08	.02	.03	.11	.12	.08	.07
.24	.24	.22	.42	.10	.09	.14	.78	.13	.17	1.14	1.30	.64	.23
1.05	1.08	2.89	.77	3.95	.27	3.07	1.95	1.01	2.29	1.32	1.05	.66	.60
.98	.89	2.00	.88	2.26	.17	2.71	1.58	.86	1.77	2.18	1.63	.90	2.74
98.51	98.51	98.51	98.50	98.49	98.48	98.49	98.51	98.49	98.50	98.51	98.50	98.50	98.49
(73.07)	(74.97)	(77.72)	(82.99)	(88.43)	(84.59)	(84.29)	(88.05)	(87.84)	(87.71)	(88.20)	(85.02)	(87.64)	(83.89)
4	5	4	2	2	2	1	8	5	3	1	1	1	1
16.4	9.7	78.6	92.2	65.5	---	43.3	82.5	---	80.0	26.9	49.4	---	79.7
77.4	78.9	14.9	3.4	27.4	∿99	49.8	9.0	∿90	14.7	51.5	32.7	39.9	15.3
1.5	1.5	1.3	2.6	0.6	0.5	0.9	4.8	0.8	1.1	7.1	7.8	---	1.4
2.1	2.0	5.1	1.7	6.4	0.4	6.0	3.7	1.9	4.2	3.7	2.7	0.6	3.5
2.7	7.9	---	---	---	---	---	---	∿7	---	10.8	7.4	59.6	---
.31	.40	.47	.42*	.47*	.35*	.31	.28	.47	.37	.35*	.35*	.54*	.47*
.33	.08	.45	.48	.52	---	.44	.46	---	.48	.29	.45	---	.47
0.91	0.83	1.93	4.14	2.14	8.39	2.89	2.53	1.45	2.36	3.58	1.23	---	2.83

Table 1 continued

Inclusion	TS27F1			Bulk
Rim Layer	IB	III inner light	III outer dark	Mtx
	29	30	31	32[3]
SiO_2	34.51	34.50	34.17	33.11
Al_2O_3	9.41	7.61	6.28	3.07
FeO[1]	26.57	27.70	28.63	31.17
MgO	22.56	23.77	22.74	21.42
CaO	1.24	1.24	1.36	2.67
K_2O	.27	.20	.18	.03
Na_2O	2.22	1.98	1.67	.44
FeS[1]	.91	.75	1.94	4.29
NiS[1]	.82	.75	1.55	2.37
Total, norm.[2]	98.51	98.50	98.52	98.57
(Orig.)	(84.28)	(89.60)	(86.02)	(98.57)
Number of Analyses	4	5	6	
AMOUNT PRESENT (%)				
Olivine	80.2	81.6	81.2	79.5
Pyroxene	3.9	4.5	4.9	10.9
Nepheline	14.0	12.3	10.3	2.7
Total Sulfides	1.8	1.6	3.6	6.9
Andradite	---	---	---	---
MOLAR FeO/FeO + MgO				
Pyroxene[4]	.46	.37	.57	.47*
Olivine	.40	.40	.41	.45
EXCESS Al_2O_3	4.80	3.39	2.82	2.07

[1]Total nickel converted to NiS; remaining sulfur reported as FeS; remaining iron reported as FeO.
[2]Totals normalized to 98.5%, the sum of the same components in the wet chemical analysis of Allende matrix shown in column 32; numbers in parentheses are the original sums prior to normalization.
[3]From Clarke *et al.* (1970), Table 3, column 5. Wet chemical analysis of Allende matrix. Analytical sum is not normalized. Total sulfur converted to FeS for purposes of comparison.
[4],*Based on actual analysis of pyroxene in the layer and inclusion in question unless marked by asterisk, which indicates an average pyroxene composition for this type of layer on other inclusions.

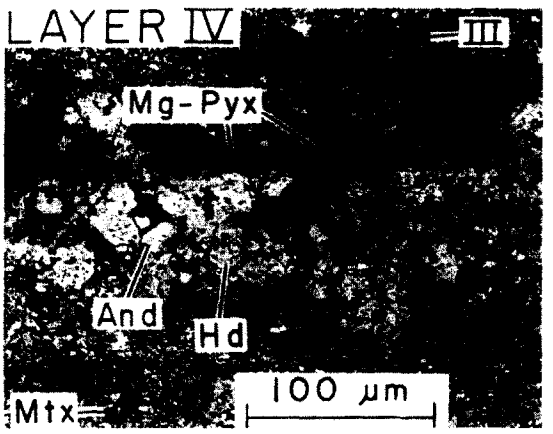

FIG. 9. Close-up b.s.e. photomicrograph of rim Layer IV on TS10F1. Clumps of blocky crystals of andradite and hedenbergite (And, Hd; both bright) are embedded in a meshwork of tiny magnesium-rich clinopyroxene needles. This layer separates Layer III from the Allende matrix. Other abbreviations as used previously.

accurate than the rastered beam technique used here, the analysis of Clarke *et al.* probably does not represent as inclusion-free a sample of the matrix as our analyses, owing to the difficulty of isolating the matrix from other fine-grained material in the meteorite. Nevertheless, in most cases, matrix analyses by the microprobe method are quite close to the wet chemical analysis.

It is clear from examination of Table 1 that the layers within a particular rim sequence have markedly different bulk compositions. In the bottom half of the table, the bulk chemical analyses are interpreted in terms of the mineral phases known to be present in each layer. In each case, all Na_2O was assumed to be present as nepheline having the average composition of that found in amoeboid olivine aggregates by GROSSMAN and STEELE (1976). In the case of matrix analyses and of Layers IB, II and III, all remaining CaO was assumed to be present as pyroxene having the average composition of 5–10 pyroxene grains analyzed in the same regions where the bulk compositions were obtained. In some cases, marked by an asterisk in Table 1, pyroxene analyses were not available for a particular layer of a particular inclusion, so the average pyroxene composition found in that type of layer on all other inclusions was used. The cation/silicon ratio of the remaining MgO, FeO and SiO_2 was within 5% of that for olivine in 14 of 23 cases, within 5–10% in six cases and within 10–12% in three cases. Thus, this material was assumed to be olivine whose concentration and molar FeO/FeO + MgO was calculated. In all cases, significantly more Al_2O_3 was present in the bulk analysis than could be accounted for by the nepheline and pyroxene known or assumed to be present. After a careful search turned up no additional aluminous phases, very fine-grained, interstitial material with a high Al_2O_3 content was discovered in the rim layers at high magnification with the SEM. We suspect that this is ground-up meteoritic material with admixed corundum grinding compound. Apparently, during grinding and polishing, significant amounts of such material can be trapped in the interstices of porous samples like these, leading to contamination of rastered or broad-beam microprobe analyses thereof. The absolute amount of this excess Al_2O_3 present in the original analyses was calculated by subtraction and is reported in Table 1. Mineral concentrations were then normalized to 100%.

In the case of Layers IA, the amounts of CaO, MgO, SiO_2 and Fe remaining after subtraction of nepheline and sulfides from the bulk analysis were used in a set of linear mass-balance equations to compute the concentrations of andradite, pyroxene and olivine that are present. Pyroxene compositions were determined as for previous layers and the olivine composition was varied until a value was found that yielded satisfactory solutions. The excess Al_2O_3 calculated as before, the mineral proportions after renormalization and the calculated olivine compositions are reported in Table 1.

Each analysis of Layer IV appears to be contaminated with material from the adjacent inner rim layer. Mass-balance equations set up as in the case of Layers IA were used to compute the concentrations of andradite and pyroxene from Layer IV and pyroxene and olivine from the contaminating layer. Pyroxene and olivine compositions were determined as previously. Assuming all olivine to be from the contaminating layer, we computed the concentrations of phases in Layer IV by subtracting out the expected amounts of all other phases in the contaminating layer and re-normalizing the results to 100%. Excess Al_2O_3 was calculated as before.

Despite the fact that, in some instances, pyroxene compositions from different inclusions had to be used for the one in question, the results of this analysis are generally in good agreement with petrographic descriptions in the previous section. Exceptions are the

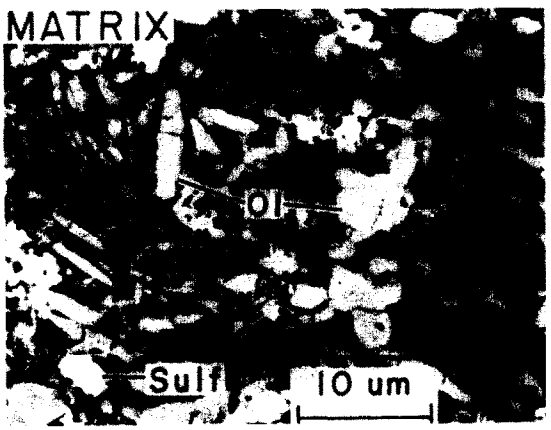

FIG. 10. Close-up b.s.e. photomicrograph of the Allende matrix. Note that the olivine crystals are plates that appear spindle-shaped in cross-section. None of these crystals have parallel edges, as they would have if they originated as pyroxene cleavage fragments. These are primary, vapor-condensed single crystals of olivine. Abbreviations as used previously.

occasional presence of unusually large amounts of olivine in Layer IA, ~50% in TS10F1, and of pyroxene in Layer IB, 30% in TS24F1 and 50% in NMNH 3643. The relatively high sulfide content and high olivine/pyroxene ratio are evident in Layer II. Andradite contents of ~40% and ~60% are indicated for Layer IV of TS19F1 and TS10F1, respectively. All of our matrix samples are richer in pyroxene than the one analyzed by CLARKE *et al.* (1970), some (TS4F1, TS25F1) by very large amounts. Overlap of the electron beam with part of Layer IV during our analyses is not a possible explanation, as our matrix samples were deliberately chosen to be far outside this layer. Perhaps CLARKE *et al.*'s sample contained enough fragments of inclusions that the assumptions we have used in calculating the mineral proportions in it are grossly in error. An indication that this may be the case is the fact that, when the CLARKE *et al.* analysis is treated like our matrix analyses, 2.07% excess Al_2O_3 results in this sample, even though there is certainly no grinding compound in it. This may be due to the presence of Al_2O_3-rich phases like spinel, grossular or gehlenite in the CLARKE *et al.* (1970) sample which are not present in ours. The excess Al_2O_3 content of Layer IA of NMNH 3643 is unusually high and, in this instance, may be due to accidental overlap of the electron beam with the adjacent Wark-Lovering rim during our analysis.

Although we have measured pyroxene compositions in relatively few examples of each type of layer, we can say that the average FeO/FeO + MgO ratio of pyroxene varies considerably from one Layer IB to another (.31–.48), one Layer III to another (.28–.57), one Layer IV to another (.47–.61) and from place to place within the matrix (.37–.58). Although this is also true of olivine for Layer IA (.08–.45), the average FeO/FeO + MgO ratio of this phase seems to vary much less than that for pyroxene from one Layer IB to another (.32–.44), one Layer III to another (.36–.48) and from place to place within the matrix (.41–.52). This may reflect the fact that average pyroxene compositions are based on analyses of relatively small numbers of pyroxene grains per layer, while average olivine compositions are calculated from bulk compositions of regions containing thousands of olivine grains and considerably less pyroxene.

Because there are only three inclusions for which we have analyzed more than two rim layers, it is difficult to determine if there are any consistent trends in the FeO/FeO + MgO ratios of olivine or pyroxene from inner to outer layers. In TS24F1, the FeO/FeO + MgO ratios of both olivine and pyroxene appear to increase progressively from the inner layers outward to and including the matrix. In TS19F1, however, the ratio for pyroxene drops from Layer II to Layer III but increases in Layer IV, while that for olivine drops slightly from II to III. In NMNH 3643, the ratio for pyroxene drops from IB to III, increases in IV and falls in the matrix, while that for olivine increases slightly from IB to III to the matrix. The FeO/FeO + MgO ratios of both olivine and pyroxene are almost always higher in the matrix outside the accretionary rims than in the outermost rim layer.

The question of why the inner rim layers are dark on slab surfaces can be addressed by considering Table 1, columns 6 and 7. The inner portion of Layer III on TS25F1 is considerably darker than the outer portion, as seen in thin section with transmitted light. Yet, as the two analyses show, there are no significant differences in the analyzed components that might account for this. Likewise, there are no significant textural and mineralogical differences. These observations suggest that dark rims may owe their color to the presence of an element not normally analyzed for by electron microprobe. Data reported by BUNCH and CHANG (1984) indicate that carbon could be this element.

DISCUSSION

Origin of the rim structures

Our interpretation of these rim structures as accretionary aggregates is based on three observations: (1) the layers are highly porous masses of euhedral crystals showing no intergrowths; (2) the layers contain highly disequilibrium mineral assemblages; and, (3) the thickness of the layers varies with underlying topography.

Although HUTCHISON and BEVAN (1983) argued for an igneous origin for dark rims on chondrules of ordinary chondrites, the absence of intergrowths in and high porosity of the rims studied here make it difficult to reconcile their origin with igneous or metamorphic processes. Crystallization of a multi-component liquid always results in a crystallization sequence that manifests itself texturally in the solidified rock as phenocrysts, dominant and subordinate crystal shapes and enclosing relationships. The only exception would be in the rare case of a eutectic composition in which all phases crystallize simultaneously but, even in this case, there is always a last bit of residual liquid that fills interstitial spaces between early-formed crystals. In the Allende rim layers, interstices are void, and neighboring crystals show no intergrowths or growth interference textures that would indicate any temporal relationships. Indeed, the extreme disequilibrium indicated by mineral compositions, as shown below, suggests that these crystals formed independently of one another under different conditions and possibly in different places. An origin by metamorphic processes is no easier to rationalize, as solid-state recrystallization in the absence of stress fields tends to produce equigranular, sugary textures with 120° triple-grain junctions and little or no porosity. It might be argued that the presently-void interstices in the rim layers were once occupied by a melt or some additional solid phase that was selectively and completely removed, presumably by dissolution in the case of a solid phase. In either case, it is hard to imagine any process so efficient but, even given that possibility, such a history would require the remaining phases in each layer to be in equilibrium with each other, which they are not.

The existence within Layers IA and IV of an assemblage whose pyroxene compositions span most of the range between diopside and hedenbergite represents an extreme degree of disequilibrium that is consistent only with formation of these rim layers by aggregation of cold, independently-formed grains. Moreover, the layers cannot have experienced any significant re-heating since they were assembled, as diffusion would have tended to smooth out the composition gradients that now exist. NORD *et al.* (1982) used scanning-transmission electron microscopy to study mineral assemblages in Wark-Lovering rims around an Allende Type A inclusion. They observed wollastonite in direct contact with hedenbergite, just as we described above in Layer IV, and pointed out that this assemblage is stable only at temperatures below 775°C. They also found single crystals of pyroxene zoned from magnesium-rich salite to hedenbergite and identical to the range present in Layers IA and IV of the accretionary rims. Those authors concluded that the process that formed such assemblages was characterized by extreme disequilibrium, and that temperatures involved were probably much lower than ~775°C. GREEN *et al.* (1971) showed on the basis of radiation damage in chondrules that Allende accretion occurred below ~230°C, and that no post-accretion re-heating had occurred. We therefore conclude that the accretionary rims were assembled below ~775°C and were not subjected to significant periods of re-heating above 230°C since assembly of the meteorite. Note that the thermal history implied by these temperature estimates is completely at odds with the model proposed by BUNCH *et al.* (1980) for the origin of the matrix of Allende as "impact comminuted material that crystallized in melt-like fashion in a post-impact ejecta sheet where temperatures of ≳600°C allowed for partial matrix melting . . .".

PECK (1983) appears to have observed some of the rim layers discussed here. Her interpretation of them as flow structures that were molded around inclusions during the thermal metamorphism proposed by BUNCH *et al.* (1980) is based upon the presence of more equant and slightly larger olivine grains than those in the Allende matrix and upon depletion of sulfur from these structures. From this description, we infer that she observed Layer IB. Other accretionary rim layers, however, have higher sulfide concentrations and tinier olivine crystals than in the Allende matrix.

The fact that accretionary rims are thickest in topographic depressions on the surfaces of inclusions and thinner or absent elsewhere on the surfaces of the same inclusions distinguishes them from Wark-Lovering rims which maintain a remarkably constant thickness around the surfaces of even the most irregularly-shaped inclusions. MACPHERSON and GROSSMAN (1984) showed that refractory inclusions underwent very little deformation subsequent to formation of Wark-Lovering rims. Since accretionary rims overlie the Wark-Lovering rims, they, too, must post-date any significant deformation. The fact that these rims are thickest in topographic depressions cannot, therefore, be explained as a consequence of mechanical folding. Perhaps the best case to be made against such a model is shown in Fig. 11, a slab surface photograph of a portion of a large (1 cm diameter) forsterite-bearing refractory inclusion (see MACPHERSON *et al.* (1981), Fig. 5a, for a photograph of the entire inclusion). The large circular re-entrant is a vesicle that was trapped in the process of escaping from the once-molten droplet just as the latter solidified. It is now filled with Allende matrix material and, on its innermost surface, a dark accretionary rim, Layer IA, which is thickest directly opposite the entrance to the cavity and pinches out completely towards the sides of the cavity. The circular shape of the vesicle and overall spheroidal shape of the inclusion rule out any deformation after the rim was emplaced, and therefore its thickness variations are primary in origin. If such rims are accretionary features, their thickness variations are consequences of the depositional processes that formed them. The most reasonable and simple interpretation is that the topographic hollows provided sheltered environments within which accreting grains were less likely to rebound away and grains that had already accreted were less likely to be dislodged by impacts of other particles.

Note that our interpretation of these features as accretionary rims is essentially the same as that adopted for "dark bands" around Allende inclusions by BUNCH and CHANG (1984) who suggested that "each object accreted a spherical mantle of fine-grained components before incorporation into a parent body".

Origin of grains in the rim layers and matrix

We have shown that the rim layers formed by accretion of independently-grown particles onto the surfaces of inclusions, but this leaves unanswered the

FIG. 11. Slab surface, incident light photomicrograph of part of the inclusion ALVIN (white in this photo). The large circular cavity is a vesicle as are smaller cavities nearby (Ves). The large cavity is filled by dark grey Allende matrix and a black layer of accretionary rim (A.R.) material on its inner surface. Other abbreviations as used previously.

question of how the grains themselves formed. According to HOUSLEY and CIRLIN (1983), Allende matrix olivine grains formed by cleavage and alteration of clinoenstatite inside chondrules. This idea is based largely on what those workers considered to be the anhedral shapes of the matrix olivine grains and they specifically attributed a different, but unspecified, origin to the olivine grains in accretionary rims because of the euhedral shapes of the latter. It is our experience, however, that the majority of olivine grains in both the Allende matrix (Fig. 10) and in rim Layer III (Fig. 7) are spindle-shaped in cross-section and do not have parallel sides as they would if they were cleavage fragments. PECK (1983) also used differences in shape between Allende matrix olivine grains and olivine crystal fragments to argue against the HOUSLEY and CIRLIN (1983) model. GREEN *et al.* (1971) showed in fact, on the basis of transmission electron microscopy, that the matrix olivine grains are euhedral single crystals elongated parallel to [001]. We thus disagree with the model proposed by Housley and Cirlin for the matrix olivine grains and consider them to have a similar origin to those in the rim layers.

As shown earlier, none of these olivine or pyroxene crystals formed *in situ* but, rather, formed independently elsewhere and were later accreted into their present sites. Either the crystals formed as parts of precursor igneous or metamorphic rocks that were completely broken up into their component crystals, or else each grain originally formed as a separate entity and was never part of something else. The former case is ruled out because no plausible process could disaggregate a rock completely into its individual component crystals without forming crystal fragments or polycrystalline aggregates, and these are not observed in either the rims or the matrix. In the second case, the crystals might have either solidified from tiny melt droplets or recrystallized in the solid state from an original amorphous material that NUTH and DONN (1983), for example, have proposed as the likely form of nebular condensates. If the crystals solidified from melt droplets, then each droplet would have had to form one euhedral crystal rather than several crystals or glass. Furthermore, each droplet would be required to have the exact stoichiometric composition of a single phase, and separate populations of droplets would be required for each phase. Such circumstances seem highly unlikely. The possibility that the crystals formed from precursor amorphous solid condensates again requires parental materials to have stoichiometric compositions of single pure phases, an idea rejected even by those who advocate condensation of amorphous solids (NUTH and DONN, 1983). On the other hand, the properties of olivine and pyroxene grains in the Allende matrix and accretionary rims are precisely those expected of condensates from a slowly cooled vapor. Their euhedral shapes suggest that they did not interfere with one another during growth and therefore were physically separate from one another at that time. Furthermore, the void spaces between them suggest that there was no condensed phase left after they crystallized. We suggest that the accretionary rims and the matrix in Allende consist mostly of condensate grains from solar nebular gas. In a structural sense, Allende and other C3's may thus be among the most pristine samples available of pre-planetary solar nebular solids.

Our observations seem readily explainable in terms of solar nebular models in which there is evaporation of most interstellar dust in the inner part of the nebula, followed by a slow cooling episode with a duration of several thousand years. This allows chemical fractionations produced during condensation to be preserved *via* dust/gas separation processes such as settling of grains toward the median plane, transport of grains in convection cells, accretion, etc. This, in turn, would allow individual inclusions to encounter and be mantled successively by assemblages with different chemical and thermal histories, resulting in rim layers with different mineral proportions and textures. Indeed, such observations as the variable sulfide contents of accretionary rim layers and the presence of hedenbergite-andradite clumps in Layers IA and IV but not in intervening layers imply that inclusions were not rimmed by materials that condensed from a simple closed system but, instead, sampled material in an intermittent fashion.

Because the FeO/FeO + MgO ratios of olivine and pyroxene vary widely from inclusion to inclusion for a given type of layer, it appears that the region of the nebula in which inclusions were mantled by a given layer contained a mineral assemblage with different FeO/FeO + MgO ratios at different times or in different sub-regions. This could have resulted, for example, from condensation of the mineral assemblage of that region at different distances from the median plane and thus at slightly different temperatures, followed by settling toward the median plane. Depending on the time or angle at which an inclusion entered the region, it could be mantled by a Layer III assemblage, say, that had the same FeO/FeO + MgO ratio, a higher one or a lower one than that which formed the previous rim layer. In a situation like this, there is no necessary reason for the FeO/FeO + MgO ratio to increase or decrease smoothly from inner to outer rim layers. Because the nebula was cooling with time, the mean FeO/FeO + MgO ratios of pyroxene and olivine were probably increasing with time in all regions. Because the rim layers represent a time sequence, it does seem possible in models like this to produce inclusions like TS24F1 in which the FeO/FeO + MgO ratios increase progressively from inner to outer rim layers.

The accretionary rims discussed here overlie the Wark-Lovering rims which MACPHERSON *et al.* (1981) attributed to reaction between the primary phases of refractory inclusions and the nebular gas. Textural evidence suggests that Wark-Lovering rim formation occurred in two stages, with introduction of Na_2O and FeO being confined to the later stage, quite possibly at a lower temperature than the first. We suggest that the last stage of Wark-Lovering rim formation occurred

prior to formation of accretionary rims or possibly even continued during accretion of the innermost layers.

Implications for parent-body accretion

A long-standing problem in understanding planet formation is the mechanism whereby small particles stuck together to form bodies whose masses were large enough to possess significant gravitational fields (*e.g.*, WEIDENSCHILLING, 1974). An important contribution by HARTMANN (1978) was the finding that, at low relative velocities, accretion becomes more probable when the accreting particles are irregular in shape, and accelerates with increasing thickness of a coating of porous rocky powder on the growing body, as these factors strongly inhibit rebound. To the extent that our interpretation of rim structures around Allende inclusions as accretionary mantles is correct, then such structures contain clues to the nature of the accretion process.

We noted earlier that the inner rim layers are thickest in topographic hollows on the surfaces of inclusions and that, beyond such surface irregularities, the outer rim layers are thicker and more continuous than the inner ones. This implies that the probability of accretion of crystals was low in the early stages of rim formation and became greater afterwards. If the encounter velocities of rim materials and inclusions were small (cm/sec), this could be interpreted in terms of Hartmann's experiments. In the early stages of accretion, rim-forming crystals would have struck the smooth, hard, rounded surfaces of inclusions and rebounded away, except where pockets tended to trap the rebounding crystals and possibly also protect them against erosion by incoming particles. Thick inner rim layers would have begun to build up in the pockets and to grow laterally beyond the pockets where they would have been thinner and less continuous. At this stage, the inclusions might have begun to encounter the material that formed the outer rim layers. Such materials would have begun to accrete preferentially on top of the earlier layers because the latter are soft, porous cushions that inhibit rebound and because they consist of interlocking meshworks of platy and needle-like crystals that readily trap incoming grains. The rim layers would have grown in depth and laterally and this, in turn, would have caused accretion to accelerate. Possibly, even the most spheroidal objects have sufficient surface irregularities that some early rim accretion could have occurred, after which accretion may have accelerated even in the case of these round inclusions. By the time the inclusions encountered the particles now comprising the Allende matrix, many of them had accretionary rims and collisions between inclusions would have been inelastic, causing clumps of inclusions and chondrules to form and possibly leading to runaway accretion in the regions of highest particle density. In this sense, the Allende matrix is merely the final rim assemblage, a super rim.

Comparison with rim structures in other meteorites

Dark rims on chondrules have been reported in a number of other meteorites, including Sharps and Hallingeberg (DODD and VAN SCHMUS, 1971), Tieschitz (CHRISTOPHE, 1976; HUTCHISON and BEVAN, 1983), Chainpur (ASHWORTH, 1977; J. S. ALLEN *et al.*, 1980), Hedjaz (ASHWORTH, 1977), Murchison (FUCHS *et al.*, 1973), Khohar, Clovis No. 1, Ngawi and Parnallee (J. S. ALLEN *et al.*, 1980), and Inman, Bishunpur, Prairie Dog Creek and Murray (KING and KING, 1981). KING and KING (1981) have reviewed many of these occurrences. Many of these were restudied by SCOTT *et al.* (1984). We have observed rims on chondrules in Semarkona and Kaba.

Because of the spheroidal shapes of most of the chondrules in ordinary chondrites, we have not been able to determine whether the rims in them are thickest in topographic depressions on the underlying surfaces, as they are for Allende inclusions. Rims on chondrules in ordinary chondrites resemble the ones in Allende only superficially. In detail, the textures are quite different. In the least equilibrated meteorites, such as Chainpur, grain sizes in the dark rims are much less than 1 μm (ASHWORTH, 1977; J. S. ALLEN *et al.*, 1980; KING and KING, 1981) and the crystals tend to be equant and polygonal in shape. Those in Allende, in contrast, contain 1–10 μm-sized, bladed or plate-like crystals. Sulfides in the same meteorites occur as unevenly-distributed, tiny dispersed grains, similar to the occurrences in Allende (J. S. ALLEN *et al.*, 1980). In the more equilibrated meteorites, however, the sulfide occurs as lace-like networks enclosing silicates and, in some cases, as massive sulfide rims (J. S. ALLEN *et al.*, 1980). These observations make it clear that only the rim structures in the very unequilibrated ordinary chondrites bear any resemblance to those in Allende.

Although our interpretation of rims in Allende as accretionary features that formed after their host inclusions solidified is the same as that of J. S. ALLEN *et al.* (1980) for those in ordinary chondrites, it is clear that rims on Allende inclusions sampled material very different from that in ordinary chondrites. It is important to emphasize that the Allende matrix itself differs from the matrix in unequilibrated ordinary chondrites in precisely the same ways as the respective rims, reinforcing our interpretation that the Allende matrix is essentially a super rim.

CONCLUSION

Because they contain disequilibrium mineral assemblages and abundant euhedral crystals with pore space between them and because their thicknesses seem to be controlled by the underlying topography of their host inclusions, the rim structures described herein are believed to be accretionary in origin. The separation of assemblages of different mineralogy, mineral-chemistry and texture into different layers seems best understood in terms of nebular models in which long, slow cooling histories allow differentiation during condensation by grain/gas separation processes. The greater thicknesses of all layers in depressions on the surfaces of inclusions and of the outer compared to the inner layers elsewhere on the surfaces of the same

inclusions suggests that the accretion probability was low at first, except in surface irregularities, but became greater later, after formation of a soft cushion of accreted crystals which may have inhibited rebound of later-accreting materials, as suggested by HARTMANN (1978).

Acknowledgements—We thank D. Appleman, R. N. Clayton, A. M. Davis, V. Ekambaram, R. Fudali and F. Richter for helpful discussions. We also thank K. Keil and E. R. D. Scott for loaning us a section of Semarkona. This research was supported by the National Aeronautics and Space Administration through grants NGR 14-001-249 and NAG 9-54 and by the National Science Foundation through grant EAR-8218154.

Editorial handling: R. Brett

REFERENCES

ALBEE A. L. and RAY L. (1970) Correction factors for electron probe microanalysis of silicates, oxides, carbonates, phosphates and sulfates. *Anal. Chem.* **42**, 1408–1414.

ALBEE A. L., QUICK J. E. and CHODOS A. A. (1977) Source and magnitude of errors in "broad-beam analysis" (DBA). *Lunar Planet. Sci. VIII*, 7–9. The Lunar Science Institute, Houston.

ALLEN J. M., GROSSMAN L., DAVIS A. M. and HUTCHEON I. D. (1978) Mineralogy, textures and mode of formation of a hibonite-bearing Allende inclusion. *Proc. Lunar Planet. Sci. Conf. 9th*, 1209–1233.

ALLEN J. M., GROSSMAN L., LEE T. and WASSERBURG G. J. (1980) Mineralogy and petrography of HAL, an isotopically-unusual Allende inclusion. *Geochim. Cosmochim. Acta* **44**, 685–699.

ALLEN J. S., NOZETTE S. and WILKENING L. (1980) A study of chondrule rims and chondrule irradiation records in unequilibrated ordinary chondrites. *Geochim. Cosmochim. Acta* **44**, 1161–1175.

ASHWORTH J. R. (1977) Matrix textures in unequilibrated ordinary chondrites. *Earth Planet. Sci. Lett.* **35**, 25–34.

BAR-MATTHEWS M., MACPHERSON G. J. and GROSSMAN L. (1979) An SEM-petrographic study of amoeboid olivine aggregates in Allende (abstract). *Meteoritics* **14**, 342.

BENCE A. E. and ALBEE A. L. (1968) Empirical correction factors for the electron microanalysis of silicates and oxides. *J. Geology* **76**, 382–403.

BUNCH T. E. and CHANG S. (1984) CAI rims and CM2 dustballs: Products of gas-grain interactions, mass transport, grain aggregation and accretion in the nebula? *Lunar Planet. Sci. XV*, 100–101. The Lunar and Planetary Institute, Houston.

BUNCH T. E., CHANG S. and OTT U. (1980) Regolith origin for Allende meteorite. *Lunar Planet. Sci. XI*, 119–121. The Lunar and Planetary Institute, Houston.

CHRISTOPHE M. (1976) La matrice noire et blanche de la chondrite de Tieschitz (H3). *Earth Planet. Sci. Lett.* **30**, 143–150.

CLARKE R. S. JR., JAROSEWICH E., MASON B., NELEN J., GÓMEZ M. and HYDE J. R. (1970) The Allende, Mexico, meteorite shower. Smithsonian Contrib. Earth Sci. No. 5.

DODD R. T. and VAN SCHMUS W. R. (1971) Dark-zoned chondrules. *Chem. Erde* **30**, 59–69.

FRULAND R. M., KING E. A. and MCKAY D. S. (1978) Allende dark inclusions. *Proc. Lunar Planet. Sci. Conf. 9th*, 1305–1329.

FUCHS L. H., OLSEN E. and JENSEN K. J. (1973) Mineralogy, mineral-chemistry, and composition of the Murchison (C2) meteorite. Smithsonian Contrib. Earth Sci. No. 10.

GREEN H. W. II, RADCLIFFE S. V. and HEUER A. H. (1971) Allende meteorite: A high-voltage electron petrographic study. *Science* **172**, 936–939.

GROSSMAN L. (1975) Petrography and mineral chemistry of Ca-rich inclusions in the Allende meteorite. *Geochim. Cosmochim. Acta* **39**, 433–454.

GROSSMAN L. and STEELE I. M. (1976) Amoeboid olivine aggregates in the Allende meteorite. *Geochim. Cosmochim. Acta* **40**, 149–155.

HARTMANN W. K. (1978) Planet formation: Mechanism of early growth. *Icarus* **33**, 50–61.

HOUSLEY R. M. and CIRLIN E. H. (1983) On the alteration of Allende chondrules and the formation of matrix. In *Chondrules and their Origins* (ed. E. A. KING), p. 145. The Lunar and Planetary Institute, Houston.

HUTCHISON R. and BEVAN A. W. R. (1983) Conditions and time of chondrule accretion. In *Chondrules and their Origins* (ed. E. A. KING), p. 162. The Lunar and Planetary Institute, Houston.

KING T. V. V. and KING E. A. (1981) Accretionary dark rims in unequilibrated chondrites. *Icarus* **48**, 460–472.

MACPHERSON G. J. and GROSSMAN L. (1981) Clastic rims on inclusions: Clues to the accretion of the Allende parent body. *Lunar Planet. Sci. XII*, 646–647. The Lunar and Planetary Institute, Houston.

MACPHERSON G. J. and GROSSMAN L. (1984) "Fluffy" Type A Ca-, Al-rich inclusions in the Allende meteorite. *Geochim. Cosmochim. Acta* **48**, 29–46.

MACPHERSON G. J., GROSSMAN L., ALLEN J. M. and BECKETT J. R. (1981) Origin of rims on coarse-grained inclusions in the Allende meteorite. *Proc. Lunar Planet. Sci. Conf. 12B*, 1079–1091.

NORD G. L. JR., HUEBNER J. S. and MCGEE J. J. (1982) Thermal history of a Type A Allende inclusion (abstract). *EOS* **63**, 462.

NUTH J. and DONN B. (1983) Nucleation theory is *not applicable* to the condensation of refractory grains in the primitive solar nebula. *Lunar Planet. Sci. XIV*, 570–571. The Lunar and Planetary Institute, Houston.

PECK J. A. (1983) An SEM petrographic study of C3(V) meteorite matrix. *Lunar Planet. Sci. XIV*, 598–599. The Lunar and Planetary Institute, Houston.

RUBIN A. E. (1984) Coarse-grained chondrule rims in type 3 chondrites. *Geochim. Cosmochim. Acta* **48**, 1779–1789.

SCOTT E. R. D., RUBIN A. E., TAYLOR G. J. and KEIL K. (1984) Matrix material in type 3 chondrites—occurrence, heterogeneity and relationship with chondrules. *Geochim. Cosmochim. Acta* **48**, 1741–1757.

WARK D. A. and LOVERING J. F. (1977) Marker events in the early evolution of the solar system: Evidence from rims on Ca-Al-rich inclusions in carbonaceous chondrites. *Proc. Lunar Sci. Conf. 8th*, 95–112.

WEIDENSCHILLING S. J. (1974) A model for accretion of the terrestrial planets. *Icarus* **22**, 426–435.